



Aluminium in the North Atlantic Ocean and the Labrador Sea (GEOTRACES GA01 section): roles of continental inputs and biogenic particle removal

Jan-Lukas Menzel Barraqueta¹, Christian Schlosser¹, H el ene Planquette², Arthur Gourain^{2,3}, Marie Cheize², Julia Boutorh², Rachel Shelley^{2,4,5}, Leonardo Contreira Pereira⁶, Martha Gledhill¹, Mark J. Hopwood¹, Fran ois Lacan⁷, Pascale Lherminier⁸, Geraldine Sarthou², and Eric P. Achterberg¹

¹GEOMAR, Helmholtz Centre for Ocean Research Kiel, Kiel, Germany

²LEMAR, UMR 6539, Plouzan e, France

³Earth, Ocean and Ecological Sciences, School of Environmental Sciences, University of Liverpool, Liverpool, UK

⁴Earth, Ocean and Atmospheric Science, Florida State University, Tallahassee, Florida, USA

⁵Geography, Earth and Environmental Sciences, University of Plymouth, Plymouth, UK

⁶Universidade Federal do Rio Grande-FURG, Rio Grande, Brazil

⁷LEGOS, Laboratoire d'Etudes en Geophysique et Oceanographie Spatiales, University of Toulouse, Toulouse, France

⁸Ifremer, Laboratoire d'Oc anographie Physique et Spatiale (LOPS), IUEM, Plouzan e, France

Correspondence: Jan-Lukas Menzel Barraqueta (jmenzel@geomar.de)

Received: 19 January 2018 – Discussion started: 23 January 2018

Revised: 17 May 2018 – Accepted: 12 June 2018 – Published: 30 August 2018

Abstract. The distribution of dissolved aluminium (dAl) in the water column of the North Atlantic and Labrador Sea was studied along GEOTRACES section GA01 to unravel the sources and sinks of this element. Surface water dAl concentrations were low (median of 2.5 nM) due to low aerosol deposition and removal by biogenic particles (i.e. phytoplankton cells). However, surface water dAl concentrations were enhanced on the Iberian and Greenland shelves (up to 30.9 nM) due to continental inputs (rivers, glacial flour, and ice melt). Dissolved Al in surface waters scaled negatively with chlorophyll *a* and biogenic silica (opal) concentrations. The abundance of diatoms exerted a significant ($p < 0.01$) control on the surface particulate Al (pAl) to dAl ratios by decreasing dAl levels and increasing pAl levels. Dissolved Al concentrations generally increased with depth and correlated strongly with silicic acid ($R^2 > 0.76$) west of the Iberian Basin, suggesting net release of dAl at depth during remineralization of sinking opal-containing particles. Enrichment of dAl at near-bottom depths was observed due to the resuspension of sediments. The highest dAl concentrations (up to 38.7 nM) were observed in Mediterranean Outflow Waters, which act as a major source of dAl to mid-depth waters of the eastern North Atlantic. This study clearly shows that the

vertical and lateral distributions of dAl in the North Atlantic differ when compared to other regions of the Atlantic and global oceans. Responsible for these large inter- and intra-basin differences are the large spatial variabilities in the main Al source, atmospheric deposition, and the main Al sink, particle scavenging by biogenic particles.

1 Introduction

Aluminium (Al) in the oceans has been used as a tracer for mineral dust deposition (Han et al., 2008; Measures and Vink, 2000; Measures and Brown, 1996) and water masses (Measures and Edmond, 1990). Aluminium is the third most abundant element in the Earth's crust (Rudnick and Gao, 2003), but concentrations of dissolved Al (dAl; filtered through 0.4 or 0.2 μm pore size filters) in the world's ocean are at nanomolar to low micromolar levels. In seawater, Al undergoes rapid hydrolysis resulting in the formation of species such as $\text{Al}(\text{OH})_3$ and $\text{Al}(\text{OH})_4^-$, which are insoluble (Roberson and Hem, 1969) and particle reactive (Orians

and Bruland, 1985), especially in association with silicon-rich particles (Moran and Moore, 1988a).

A major source of Al to the surface ocean is dry atmospheric deposition of terrigenous material (Kramer et al., 2004; Measures et al., 2005; Orians and Bruland, 1986), which can be carried thousands of kilometres in the atmosphere before deposition into the ocean (Duce et al., 1991; Prospero and Carlson, 1972). Wet atmospheric deposition (rain, fog, and snow) also plays an important role in supplying Al to both the North Atlantic (Schlosser et al., 2014; Shelley et al., 2017) and the global ocean (Guerzoni et al., 1997; Vink and Measures, 2001). Glacial runoff has been reported as a pronounced source for Arctic and Antarctic surface waters (Brown et al., 2010; Statham et al., 2008), but its impact beyond the immediate source regions has not yet been established. Fluvial inputs were historically considered a dominant source of Al to the surface ocean (Stoffyn and Mackenzie, 1982), but Al removal through particle scavenging during estuarine mixing processes appears to strongly reduce the riverine Al outflows (Hydes, 1989). However, recent publications have indicated significant fluvial sources for Al (Brown and Bruland, 2009; Brown et al., 2010; Grand et al., 2015). Sediment resuspension represents an important source of Al to the deep ocean, especially along ocean margins with strong boundary currents (Jeandel et al., 2011) and in areas with benthic nepheloid layers (Middag et al., 2015b; Moran and Moore, 1991). Recently, hydrothermal vents (Measures et al., 2015; Resing et al., 2015) were noted as Al sources to the deep Atlantic and Pacific oceans, with plumes extending at depth over 3000 km in the Pacific Ocean.

Removal of Al in oceanic waters occurs through particle scavenging with subsequent sinking of the particulate matter (Orians and Bruland, 1986). This removal occurs via both active and passive scavenging processes. Active scavenging occurs when dAl is incorporated into the atomic structure of opaline diatom frustules, a process which has been demonstrated in laboratory experiments and is also supported by positive correlations between silicic acid ($\text{Si}(\text{OH})_4$) and Al in depth profiles as a result of the sinking and remineralization of diatomous material (Gehlen et al., 2002; Hydes et al., 1988; Hydes, 1989; Middag et al., 2009, 2015b; Moran and Moore, 1988a). Passive scavenging is defined as dAl being adsorbed onto any particle surface without being intrinsically incorporated into cellular structures. This is inclusive of adsorption onto biogenic particles. Evidence for post-mortem incorporation (e.g. passive scavenging) of Al into diatoms frustules and concomitant removal from the dissolved phase is given by Koning et al. (2007) and Vrieling et al. (1999).

In the North Atlantic (specifically 40–65° N) vertical dAl profiles combined with high-resolution sections were scarce prior to the GEOTRACES era (Mawji et al., 2015). In the western North Atlantic, reported dAl concentrations range from 1 nM in surface waters to 27 nM near the seafloor (Hall and Measures, 1998; Middag et al., 2015b). In the eastern North Atlantic, dAl concentrations in surface wa-

ters range between 1–5 nM (Measures et al., 2008), and a dAl mid-depth maximum (> 30 nM) is observed associated with Mediterranean Outflow Waters (MOW; Measures et al., 2015; Rolison et al., 2015). Globally, the highest dAl concentrations have been measured in the Mediterranean Sea (up to 174 nM; Chou and Wollast, 1997; Hydes et al., 1988; Rolison et al., 2015) and the subtropical North Atlantic (up to 60 nM; Schlosser et al., 2014), while the lowest concentrations (< 1 nM) were found in the Southern Ocean (Middag et al., 2011), the Pacific Ocean (Orians and Bruland, 1986), and the high-latitude North Atlantic (Middag et al., 2015b).

This manuscript provides an overview of the surface and water column distribution of dAl in the North Atlantic Ocean and Labrador Sea along GEOTRACES section GA01. The sources and sinks of Al for the surface and deep ocean are discussed, and the controls that regulate dAl are examined in light of $\text{Si}(\text{OH})_4$ and particulate Al (pAl) distributions.

2 Methods

2.1 Sampling and processing

The GEOVIDE cruise was conducted as part of the GEOTRACES programme (GA01 section), and sailed on 15 May (2014) from Lisbon (Portugal), passed by the southern tip of Greenland (16, 17 June), and arrived in St. John's (Canada) on 30 June (Fig. 1a). A total of 32 stations were sampled for dissolved and particulate trace metals. Seawater was collected using a trace metal clean rosette (TMR, General Oceanics Inc. model 1018 intelligent rosette) attached to a Kevlar line and fitted with 24×12 L GO-FLO bottles (General Oceanics). After recovery, GO-FLO bottles were transferred to a clean container for sampling.

Dissolved Al samples were filtered using 0.2 μm capsule filters (Sartobran 300, Sartorius) or 0.45 μm polyethersulfone filters (Supor[®], Pall Gelman), under a slight overpressure (0.2 bar; filtered, Acrovent, N₂, Air Liquide). Seawater samples were collected in 125 mL low-density polyethylene bottles (LDPE; Nalgene) and cleaned using a three-step protocol (as per GEOTRACES cookbook; <http://www.geotraces.org>, last access: 17 September 2017). After collection, the samples were acidified to pH 1.8 with HCl (ultra-pure acid, UpA; Romil) and double bagged. Samples were then stored upright in order to minimize contact and potential contamination arising from the polypropylene caps. Samples were shipped to GEOMAR (Kiel, Germany) and analysed in a class 100 clean laboratory. Samples for particulate trace metals (Gourain et al., 2018) were collected on 0.45 μm pore size polyethersulfone (PES) filters (Supor[®], Pall Gelman) and stored frozen until analysis at LEMAR (Brest, France). Additionally, total dissolvable Al (tdAl) samples (unfiltered) were collected (May 2014) by hand in 125 mL acid-cleaned LDPE bottles (Nalgene) from icebergs ($n = 11$) and surface waters in Godthåbsfjord ($n = 6$; SW Greenland), acidified

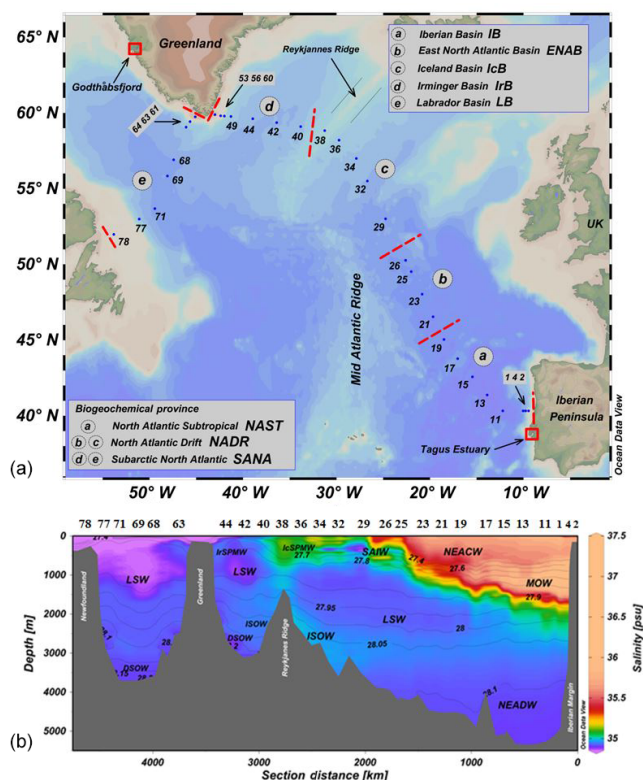


Figure 1. (a) The cruise track along the North Atlantic and the Labrador Sea. (b) Cross-section plot of salinity along GEOVIDE. Annotations represent main water masses in the study region. Iso-lines represent layers of equal neutral density (σ^{θ}). DSW, Denmark Strait Overflow Water; ISOW, Iceland Scotland Overflow Water; LSW, Labrador Sea Water; MOW, Mediterranean Outflow Water; NEACW, North East Atlantic Central Water; NEADW, North East Atlantic Deep Water; IcSPMW, Iceland Sub-Polar Mode Water; IrSPMW, Irminger Sub-Polar Mode Water; SAIW, Sub-Arctic Intermediate Water. Plots created in Ocean Data View (Schlitzer, 2018).

to pH 1.8 by addition of HCl (UpA, Romil), and stored for 6 months prior to analysis at GEOMAR. After collection, ice samples were defrosted at room temperature in LDPE bags, with the first meltwater discarded to minimize contamination from sample collection, as described by Hopwood et al. (2016).

2.2 Dissolved Al analysis

Dissolved seawater samples were analysed using flow injection analysis (FIA) with fluorescence detection as developed by Resing and Measures (1994), and modified by Brown and Bruland (2008). A slight modification of the method published by Brown and Bruland (2008) is the use of a 2 M ammonium acetate buffer instead of a 4 M buffer in the reaction stream. In short, acidified samples were buffered on-line to pH 5.1 ± 0.1 with a 2 M ammonium acetate buffer

(UpA, Romil), and passed over a chelating iminodiacetic acid resin (Toyopearl AF-Chelate 650M). The loading time was normally adjusted to 120 s (2.5 mL min^{-1}) and was extended up to 180 s for samples with low dAl concentrations ($< 2 \text{ nM}$). After sample loading, the column was rinsed for 70 s (2.5 mL min^{-1}) with deionized water ($18.2 \text{ M}\Omega \text{ cm}$, Milli-Q, Millipore) to remove the seawater matrix which interferes with the analysis. Subsequently, the preconcentrated dAl was eluted (120 s , 0.6 mL min^{-1}) from the resin using 0.1 M HCl solution (UpA, Romil) and passed into the reaction stream. Next, the eluent was combined with lumogallion (TCI) in 2 M ammonium acetate buffer. The eluent and lumogallion mixture was passed through a 5 m long reaction coil with external heating to 60°C , supporting the formation of the fluorescent complex. After that, the reagent stream was combined with a 2.5 % (volume: volume deionized water) Brij 35 % solution (Sigma Aldrich) prior to detection using a fluorometer (Shimadzu RF-10A XL). Emission and excitation wavelengths were set to 484 and 502 nm, respectively. All samples were analysed in duplicate and the concentrations calculated using fluorescence peak heights.

Calibration was undertaken using standard additions prepared in low trace metal seawater. The different standards were prepared from a stock standard solution of $1 \mu\text{M}$ prepared from a 1000 ppm Al standard (Merck Millipore). Typically, a calibration was set up with the following standard additions: 0, 2, 4, 12, 20, and 30 nM. The buffer blank was determined as the difference in counts (arbitrary units) between three identical samples treated with increasing amounts of buffer (single, double, and triple buffer addition). The system manifold blank was determined as the mean value of two acidified (pH 1.8) samples analysed without buffering. The total blank contribution was calculated as the sum of the buffer and the manifold blank. The total blank (mean = $0.23 \text{ nM} \pm 0.1 \text{ nM}$; $n = 28$) was subtracted from the results obtained. The detection limit (0.4 nM) was calculated as 3 times the standard deviation of the manifold blank.

The accuracy and precision of the measurements were evaluated by analysis of consensus seawater samples as well as internal reference seawater. GEOTRACES deep (GD) and SaFe S reference seawater were analysed ($n = 4$ and $n = 9$) yielding an average concentration of 17.79 ± 0.26 and $1.85 \pm 0.33 \text{ nM}$, respectively, and were in good agreement with the GEOTRACES consensus values as of May 2013 (<http://www.geotraces.org>; SaFe S = $1.67 \pm 0.1 \text{ nM}$; GD = $17.7 \pm 0.2 \text{ nM}$). A second validation approach of the results was obtained by the comparison of two stations sampled in close proximity in the Iberian Basin by the GEOVIDE cruise (station 11; 40.33° N , 12.22° W) and the GEOTRACES section GA04N (station 1; 39.73° N , 14.17° W ; Rolison et al., 2015). Dissolved Al was analysed, based on the same method, using similar analytical techniques in different labs. It is noteworthy that samples for dAl during GA04N and GA01 were analysed at sea and on shore, respectively. Samples analysed for GA01 were stored upright

in order to minimize any contact and potential contamination arising from the polypropylene caps. The dAl data from waters deeper than 1000 m were used to exclude seasonal variations and based on the salinity profiles which matched below this depth. The Fisher's exact test was used for comparison between profiles as both flow injection datasets were measured with replicates (Middag et al., 2015a). This test calculates an integrated p value as an objective metric to determine how far two profiles are consistent between each other within a given depth interval. The test determined no significant difference (i - p value = 0.2–0.3) within analytical uncertainty comparing the two profiles. The dAl dataset has thus been successfully intercalibrated through GEOTRACES, included in the Intermediate Data Product 2017 (Schlitzer et al., 2018) and submitted to the British Oceanographic Data Centre (BODC; <https://www.bodc.ac.uk/>, last access: 7 September 2017).

2.3 Ancillary data

Suspended particles were digested at LEMAR following the protocol of Planquette and Sherrell (2012) and analysed for pAl exactly as described in Gourain et al. (2018). Silicic acid concentrations were analysed on board using a Bran + Luebbe AA III autoanalyser following Aminot and K erouel (2007).

A SeaBird sensor package 911 mounted to the CTD frame recorded pressure, temperature, and salinity data, while a SeaBird 43 was used for dissolved oxygen. Salinity and oxygen data were calibrated using analysis of discrete samples with a salinometer (Guildline) and the Winkler method (Carpenter, 1965), respectively.

3 Results and discussion

3.1 Regional and hydrographical settings

Along the GEOVIDE section, three biogeochemical provinces defined by Longhurst (2010) were studied: (i) the North Atlantic Subtropical (NAST) region, including the Iberian Basin (IB, stations 1 to 19); (ii) the North Atlantic Drift (NADR) region, including the Eastern North Atlantic Basin (ENAB, stations 21 to 26), and the Iceland Basin (IcB, stations 29 to 38); (iii) the subarctic North Atlantic (SANA), including the Irminger Basin (IrB, stations 40 to 60) and the Labrador Basin (LB, stations 61 to 71) (Fig. 1a). The salinity distribution and the main water masses in the North Atlantic and Labrador Sea are shown in Fig. 1b. The main water masses used in the discussion of the dAl distribution are the (i) MOW which originates in the Mediterranean Sea, is present at intermediate layers (~ 500 to 2600 m) on the most eastern part of the section, and decreases in salinity and density with increasing distance from Gibraltar (Baringer and Price, 1997); (ii) Iceland Scotland Overflow Waters and Denmark Strait Overflow Waters (ISOW and

DSOW, respectively) which are cold and saline water masses (ISOW has θ of 2.6 °C, S of 34.98; DSOW has θ of 1.3 °C, S of 34.90) formed in the Norwegian and Nordic seas and produced during the overflow across the sills in the Faroe Bank Channel and the Iceland–Faroe ridge for the ISOW, and across the Denmark Strait into the IrB for the DSOW (Read, 2000; Swift et al., 1980; Tanhua et al., 2005; Van Aken and De Boer, 1995); (iii) North East Atlantic Central Water, which originates in the North Atlantic subtropical gyre by subduction of surface waters (Pollard et al., 1996); (iv) North East Atlantic Deep Water (NEADW), which is enriched in $\text{Si}(\text{OH})_4$ and NO_3^- and is depleted in O_2 ; and (v) Labrador Sea Water (LSW) which is formed by freshening, cooling and deep convection of the subpolar mode water in the Labrador Sea (Talley and McCartney, 1982). A detailed description of the water masses and mixing figures, obtained through an extended optimum multiple parameter (eOMP) analysis can be found in Garc a-Ib a nez et al. (2018).

3.2 The surface distribution of dAl along the GEOVIDE transect: influences of atmospheric deposition, phytoplankton community structure, and freshwater sources

Figure 2 shows average dAl concentrations in surface waters (> 50 m depth) along the cruise track, except for stations above the Iberian and Greenland shelves. The latter stations are shown in Figs. 3 and 4. Dissolved Al concentrations ranged between 0.54 (station 26) and 30.99 nM (station 2). Average surface dAl concentrations decreased from 3.3 ± 1.7 nM ($n = 5$) in the IB (stations 1, 2, and 4 are excluded due to elevated dAl concentrations from inputs by the Tagus estuary) to 3.2 ± 0.8 nM ($n = 4$) in the ENAB (stations 21 to 26), and 2.8 ± 1.2 nM ($n = 5$) in the IcB (stations 29 to 38) to 1.7 ± 0.7 nM ($n = 4$) and 1.7 ± 0.6 nM ($n = 3$) in the IrB and LB (stations 53, 56, 60, 61, and 64 are excluded due to elevated dAl concentrations related to inputs from Greenland), respectively. However, within analytical errors, no significant difference was observed between basins. Our low surface dAl values agreed with literature values for the ENAB (Barrett et al., 2015; Kramer et al., 2004; Measures et al., 2008; Ussher et al., 2013) and IrB (Middag et al., 2015b), and coincided with low pAl concentrations (Gourain et al., 2018) except over the Greenland shelf (see Sect. 3.2.4; Fig. 4).

3.2.1 Atmospheric deposition

In the North Atlantic atmospheric aerosol loading declined, in a northwestward direction, with increasing distance from African dust source regions (e.g. Sahara and Sahel; Duce et al., 1991; Jickells et al., 2005). The low dAl surface concentrations observed (Fig. 2) in the different basins suggest a low aerosol deposition to the study area, which is consistent with low aerosol deposition fluxes reported for the

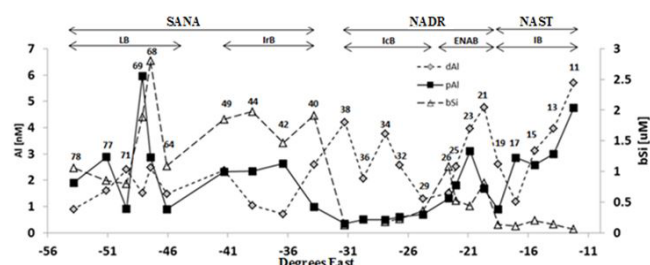


Figure 2. Average surface distribution (< 50 m) of dissolved Al (dAl), particulate Al (pAl; Gourain et al., 2018), and biogenic Si (bSi; Sarthou et al., 2018) along the GEOVIDE section. Note that stations over the Iberian and Greenland shelves are not included as they are presented in Figs. 3 and 4. LB, Labrador Basin; IrB, Irminger Basin; IcB, Iceland Basin; ENAB, East North Atlantic Basin; IB, Iberian Basin; SANA, Subarctic North Atlantic; NADR, North Atlantic Drift; NAST, North Atlantic Subtropical.

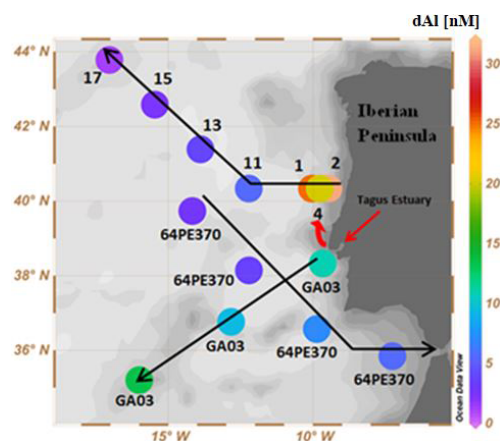


Figure 3. Surface concentration of dAl in the Iberian Basin during GEOVIDE. Label GA03 refers to GEOTRACES section GA03 (Measures et al., 2015); 64PE370 refers to GEOTRACES section GA04N (Rolison et al., 2015). Black arrows show the cruise tracks. Red arrows show the location of the Tagus estuary and the northward direction of the Tagus plume. Plot created in Ocean Data View (Schlitzer, 2018).

GEOVIDE cruise by Shelley et al. (2017) and Menzel Barraqueta et al. (2018). Aerosol deposition is considered as a major source of Al to the surface ocean and modelling studies on global dust deposition indicate a 10-fold decrease in atmospheric dust deposition fluxes between Portugal and the Labrador Sea (~ 5 to 0.5 g m⁻² yr⁻¹, values from Mahowald et al., 2005) (Han et al., 2008; Jickells et al., 2005; Mahowald et al., 2005; van Hulst et al., 2014, 2013). We performed a one-way ANOVA analysis of surface dAl and pAl for the different basins to determine whether atmospheric deposition was the dominant control on surface Al distributions, expecting a decrease in concentrations from east to west. However, no significance difference was observed (at the *p* < 0.05 level) in surface dAl and pAl between the different basins

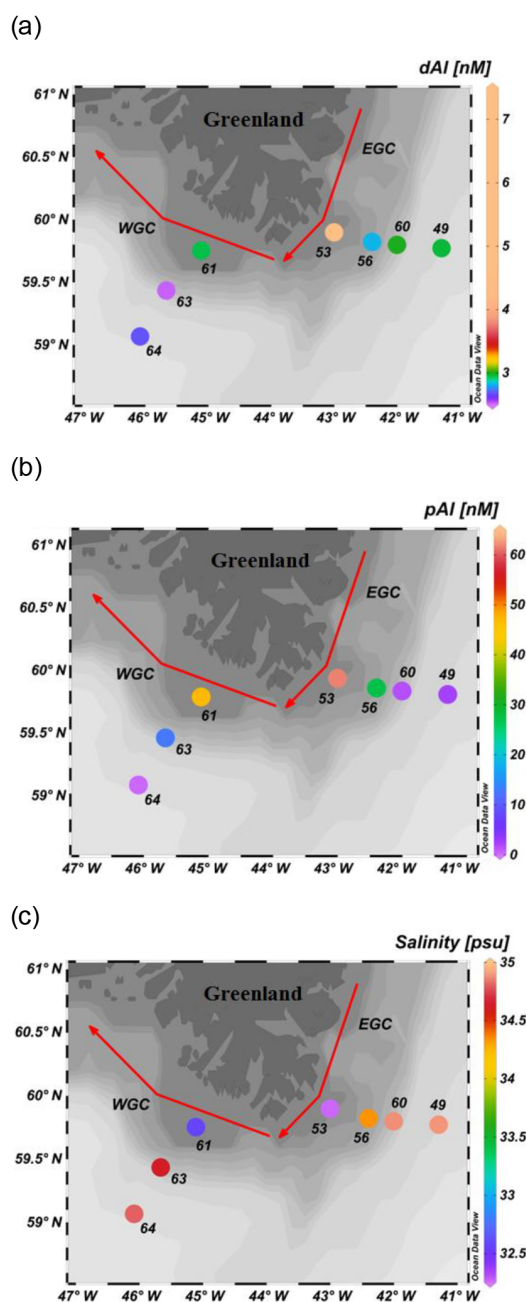


Figure 4. Surface concentration around the southern tip of Greenland of: (a) dAl (nM); (b) pAl (nM; Gourain et al., 2018); and (c) Salinity (psu). Red arrows represent the main surface currents. EGC and WGC stand for the East Greenland Current and West Greenland Current, respectively. Plots created in Ocean Data View (Schlitzer, 2018).

(dAl: [*F*(3, 17) = 0.89, *p* = 0.46]; pAl: [*F*(3, 17) = 1.79, *p* = 0.18]). Hence additional processes must have controlled the surface distribution of Al along the section (see following sections).

3.2.2 Dynamic equilibrium between dissolved and particulate Al phases

Biogenic opal production and biogenic particles play an important role in the removal of dAl in the surface ocean as a result of the high particle surface affinity of dAl (Moran and Moore, 1988b). Removal of dAl by particles therefore represents a mechanism which reduces dAl and increases pAl concentrations in surface waters (Moran and Moore, 1988a). During the GEOVIDE cruise, Chl *a* concentrations increased from the NAST (0.2 to 0.6 mg m⁻³), via the NADR (0.5 to 1.3 mg m⁻³), to the SANA region (up to 5.5 mg m⁻³ at station 61) (Tonnard et al., 2018b). Along the GEOVIDE transect, diatoms were the dominant phytoplankton taxa (> 40 % of total phytoplankton community) in the ENAB, IrB, and LB, while coccolithophorids were dominant (~ 50 % of total phytoplankton community) in the IcB (Tonnard et al., 2018b). Elevated biogenic Si (bSi; Sarthou et al., 2018) and pAl concentrations (Gourain et al., 2018) and low dAl concentrations coincided with diatom-dominated phytoplankton communities for the ENAB, IrB, and LB (Fig. 2). In contrast, elevated dAl and low bSi and pAl concentrations coincided with coccolithophore-dominated phytoplankton communities for the IcB (Fig. 2). The latter could suggest a preferential scavenging of dAl by diatoms rather than by coccolithophorids. This conclusion is supported by increased pAl to dAl ratios where surface waters were dominated by diatoms (Fig. 5), as possibly a consequence of active dAl incorporation into siliceous shells (Gehlen et al., 2002) or scavenging of dAl onto biogenic opal (Moran and Moore, 1988a). One-way ANOVA analysis was performed for the pAl to dAl ratio in the surface waters (> 50 m) in each of the four basins which showed strong dAl to Si(OH)₄ correlations with depth (LB, IrB, IcB, and ENAB, see Sect. 3.3). The ANOVA test showed significant differences (at the $p < 0.01$ level) between basins [$F(3, 38) = 7.9$, $p = 0.0003$]. Post hoc comparisons using the Tukey HSD (honestly significant difference) test showed significant differences between the LB and IcB ($p < 0.01$) or ENAB ($p < 0.05$), and between the IrB and IcB ($p < 0.01$). No significant difference was observed between the IrB and LB or ENAB ($p = 0.86$ and 0.28 , respectively), and between ENAB and IcB ($p = 0.3$). Taken together, our results indicate that when diatoms were abundant, as in the IrB and LB (> 60 % of total phytoplankton community; Tonnard et al., 2018b), the ratio between pAl and dAl significantly increases due to dAl sorption onto biogenic opal surfaces and the transfer of Al from the dissolved to the particulate fraction. Similar observations have been reported for laboratory studies and in the field where dAl decreased as a function of diatom growth and/or the presence of enhanced quantities of biogenic particles (Hydes, 1979; Kremling, 1985; Kremling and Hydes, 1988; Measures et al., 1986, 1984; Orians and Bruland, 1986; Stoffyn, 1979; van Bennekom, 1981). In addition, the transfer from dAl to pAl has been observed in coastal regions (Brown et al., 2010;

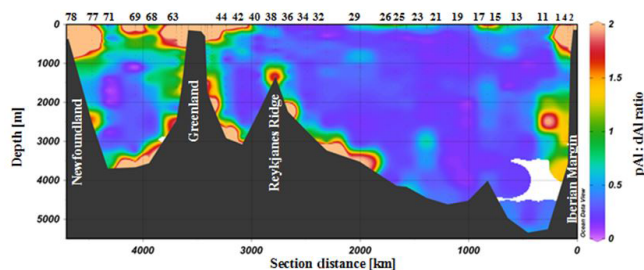


Figure 5. Cross-section plot of the pAl to dAl ratio (mol : mol) over the full depth of the water column. Plots created in Ocean Data View (Schlitzer, 2018).

Moran and Moore, 1988a) and the North Atlantic (Barrett et al., 2015). Considering the low aerosol deposition, reduced fluvial inputs into the tested basins (ENAB, IcB, IrB, and LB), and elevated levels of bSi, we conclude that the observed differences in pAl to dAl ratios were mainly related to diatom abundance.

3.2.3 The Iberian shelf surface waters: influence of the Tagus estuary

Enhanced surface water (ca. 15 m) dAl concentrations were observed on the Iberian shelf (stations 1, 2, and 4), with average dAl concentrations of 25.5 ± 5.5 nM ($n = 3$; Fig. 3) that decreased westwards, reaching 5.6 nM at station 11 (Fig. 3). Previous GEOTRACES cruises close to the Iberian Peninsula, GA03 (Measures et al., 2015) and GA04N (Rolison et al., 2015), observed average surface water dAl concentrations of 11.1 ± 2 nM ($n = 3$) and 4.7 ± 2 nM ($n = 4$), respectively (Fig. 3). Higher surface dAl concentrations were observed for the GA01 than for the GA03 or GA04N cruises, despite atmospheric aerosol deposition of Al being 1 order of magnitude lower during GA01 compared to GA03 (Shelley et al., 2015, 2017). Possible sources which could explain the elevated surface dAl concentrations are shelf sediment resuspension, wet deposition, and riverine inputs. Shelf sediment resuspension is unlikely to be the reason for the elevated dAl concentrations as deep profiles for stations 2 and 4 (Fig. S1 in the Supplement) showed that the elevated levels of dAl observed in bottom waters were not a source for surface waters since minimum dAl values were observed between maximum surface and deep dAl values. Salinity profiles for GEOVIDE showed salinity minima (< 35) in surface water for stations 1, 2, and 4 (Fig. S2), indicating a freshwater source. No evidence of freshwater input was observed at station 11, located just west of station of 1. Plausible explanations for the observed distribution in salinity are therefore wet deposition and/or river inputs. Wet deposition events were registered between stations 1 and 4 (Shelley et al., 2017). Yet, the shape of the salinity profiles of stations 1 to 4 seem unlikely to have been caused solely by recent wet deposition as the differences in salinity were observed up to a depth of 45 m.

Table 1. Correlations between salinity (S) and dAl and pAl for the eastern and western transects off Greenland. Endmember salinity 0 estimations for dAl and pAl.

Transect	Correlation S vs. dAl	R^2	Correlation S vs. pAl	R^2	Endmember $S = 0$ dAl – pAl (nM)
Eastern flank	dAl = $-1.6586S + 60.5$	0.94	pAl = $-22.018S + 773.7$	0.95	$60.5 \pm 9.9 - 773.7 \pm 125.6$
Western flank	dAl = $-0.1013S + 6.2$	0.89	pAl = $-19.272S + 675.1$	0.97	$6.2 \pm 1.2 - 675.1 \pm 124.7$

The ADCP data from cruise GA01 (Fig. S3) showed that surface waters near the Iberian Peninsula flowed in a northward direction. Therefore, we suggest that the additional source of dAl to surface waters originated from the Tagus estuary located approximately 175 km south from stations 1, 2, and 4. Elevated concentrations of dissolved Fe in the Tagus outflow and strong correlations for salinity against dAl and dFe (Tonard et al., 2018a) observed during the GA01 cruise supports a riverine source of dAl. However, we note that the wet deposition events registered between stations 1 and 4 during the GA01 cruise (Shelley et al., 2017) formed an additional freshwater source of dAl to surface waters which was superimposed on the Tagus input. Our results indicate that a fraction of riverine dAl can be advected offshore, as observed previously in the Bay of Bengal (Grand et al., 2015), Gulf of Alaska (Brown et al., 2010), and coastal waters of Oregon and Washington (Brown and Bruland, 2009), despite removal of dAl in estuaries (Hydes, 1979; Maring and Duce, 1987).

3.2.4 The Greenland shelf surface waters: influence of glacial runoff and ice melt

Concentrations of dAl in surface water samples collected on the Greenland shelf ranged between 2 and 7 nM, and coincided with reduced salinities (down to 32.2) and enhanced pAl concentrations (up to 62 nM; Fig. 4 a, b, and c). Linear regressions between dAl, pAl, and salinity for surface samples collected SE and SW of Greenland had coefficients of $R^2 > 0.89$ (Table 1). Aluminium concentrations increased with reduced salinity, potentially indicating a freshwater Al source (ice melt, glacial runoff, or sea-ice melt). However, as was the case for the Iberian Shelf, it is challenging to distinguish between multiple terrestrially derived dAl sources which co-occur in near-shore waters. Both, sea-ice melt and a smaller fraction of runoff (inclusive of tundra runoff, glacial discharge, and meltwater from calved ice) are delivered by the East Greenland Current (EGC), which flows southwards parallel to the eastern coast of Greenland (Bacon et al., 2002; Martin and Wadhams, 1999; Woodgate et al., 1999).

Freshwater endmembers (salinity 0) for Al were determined from linear regressions between dAl, pAl, and salinity for the eastern stations (49, 53, 56, and 60; dAl 60.5 ± 9.9 nM; and pAl 773.7 ± 125.6 nM) and western stations (61, 63, and 64; dAl 6.2 ± 1.2 nM; and pAl 675.1 ± 124.7 nM) on the Greenland shelf (Table 1). These endmember estimates will be considered conservative as they do not incorporate

Al scavenging processes. To gain some insight into what sources may have contributed most strongly to our high Al signals in surface waters off the Greenland shelf, we analysed a collection of iceberg and fjord samples from west Greenland. Mean total dissolvable Al (unfiltered) iceberg and fjord concentrations were 55 ± 2 nM and 12.8 ± 6 μ M, respectively (Table S1). Freshwater Al endmembers (dAl + pAl) derived from our shelf stations were 1 order of magnitude higher than the mean tdAl measured in iceberg samples. The tdAl must by definition be less than pAl due to the weaker leaching procedure applied. Yet given the large difference, the Al values off Greenland appear to be related to the input from terrestrial runoff enriched with glacially derived sediment, with this enrichment occurring either downstream of glaciers in pro-glacial environments or in near-shore environments where sediment plumes can result in high trace-element concentrations throughout the year (Hopwood et al., 2016). This is consistent with a similar elevated Fe signal on the Greenland shelf. Similar observations of elevated Al were made downstream of a glacier catchment in Cumberland Bay (Schlosser et al., 2017), and attributed to suspended glacial flour as the main source for enhanced pAl concentrations. An alternative low salinity dAl signal could come from sea ice, which contributes a total freshwater input to the EGC approximately equal to that of terrestrial runoff (Sutherland et al., 2009). Whilst sea ice dAl concentrations are not available for this study region, Lannuzel et al. (2011) reported median dAl and pAl concentrations in sea ice (pack ice) of 2.6 and 10.7 nmol L^{-1} , respectively. We therefore anticipate that local ice-melt (from sea ice and icebergs) formed a minor contributor to the shelf dAl signal compared to terrestrial runoff.

3.3 Overview of the water column distribution of dAl

The section of dAl showed low concentrations in surface waters and an increase with depth (Fig. 6a, b, c), therefore resembling a nutrient-type distribution. The IB formed an exception with maximum dAl (up to 38 nM) observed at intermediate depths associated with the MOW (Fig. 6a, b, c and Fig. S4; see Sect. 3.4.1). Average dAl depth profiles as well as maximum, minimum, median, and quartile (1st and 3rd) dAl values per basin are presented in Fig. 6b. In subsurface waters between 50 and 500 m depth the median dAl concentrations were lowest in the LB (4.3 nM) and highest in the ENAB (7.6 nM) associated with North East Atlantic Central

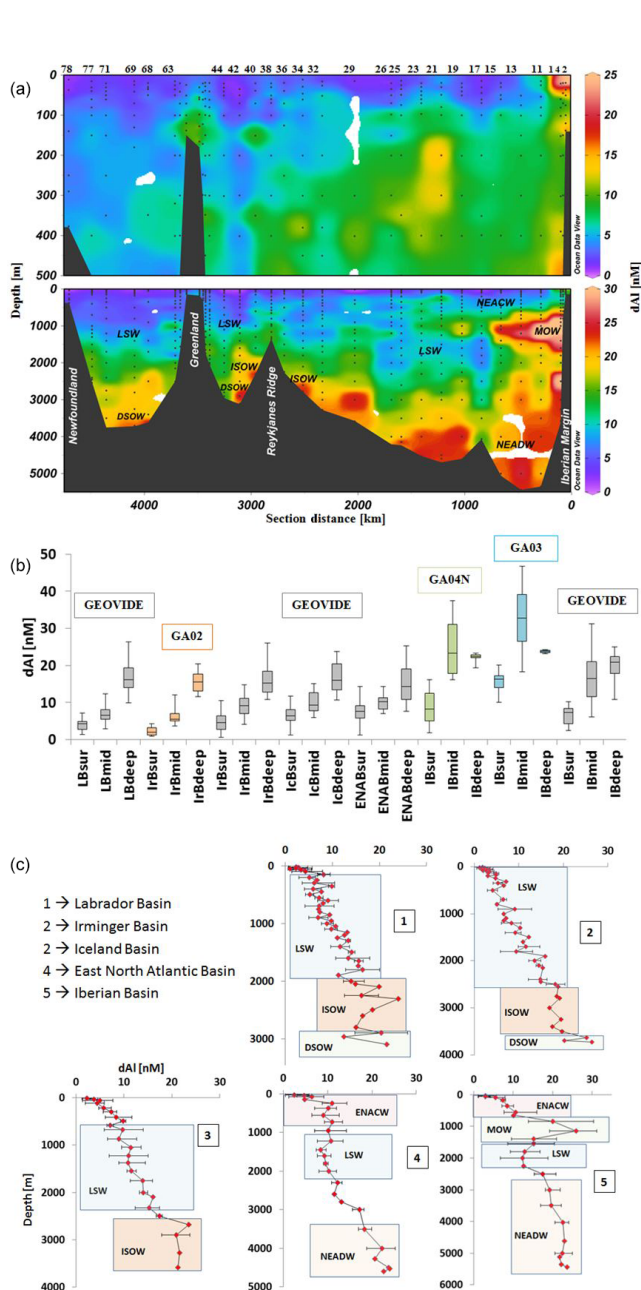


Figure 6. (a) Cross-section plot of dAl concentrations (nM) over the full depth of the water column. Numbers represent the station numbers. On the Greenland shelf, station numbers are as follows: from right to left 49, 60, 56, 53, 61, 63, and 64. Discrete sampling depths are indicated by filled black dots. For reference to water masses, please refer to Fig. 1b. (b) Box and whisker plots for the different basins relative to depth. Sur: 50–500 m; Mid: 500–2500 m; Deep: 2500 m–seafloor. Note that for the IrB and LB, sur, mid, and deep stand for 50–300, 300–1500, and 1500 m–seafloor as these basins are less deep. Orange, green, and blue boxes are data from GEOTRACES cruise GA02 (Middag et al., 2015b), GA04N (Rolison et al., 2015), and GA03 (Measures et al., 2015), respectively. (c) Average dAl depth profiles (see Sect. 3.1 for stations).

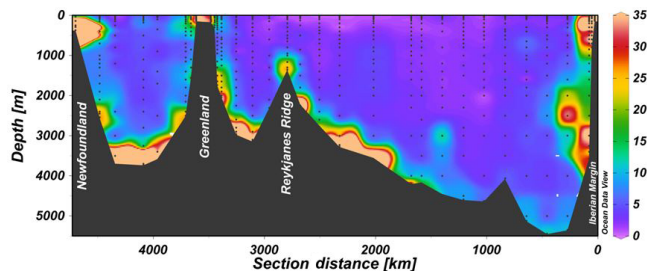


Figure 7. Section plot of particulate Al along the GEOVIDE section. For station numbers, please refer to Fig. 6. Data are from Gourain et al. (2018).

Waters (Fig. 6c), with an overall median concentration along the full transect of 5.9 nM ($n = 132$). Figure 7 displays the pAl section for the GEOVIDE cruise. In the IB, observed dAl in subsurface waters compare well with GEOTRACES GA04N (Rolison et al., 2015; median 7.3 nM for GA01 and 8.2 nM for GA04N), although they are lower than for GA03 (Measures et al., 2015; median 16.4 nM; Fig. 6b). GA01 and GA04N cruises sampled the region in May 2015 and May 2013, respectively, while GA03 sampled in October 2010. The region is known to receive enhanced atmospheric aerosol deposition (Mahowald et al., 2005). A possible explanation for the difference between GA01 and GA04N with GA03 may be that dAl is accumulated in surface waters during June to September; thus, following the late summer–autumn bloom in the Iberian Basin, it is possible that the excess of dAl accumulated in surface waters is removed by particles produced by the bloom and then released in subsurface waters. However, this explanation remains speculative. Subsurface dAl in the IrB compared well with the GA02 data (Middag et al., 2015b; Fig. 6b). In deep waters, sampled between 500 and 2500 m, the median dAl concentration was lowest in the LB (6.6 nM) and highest in the IB (15.7 nM), with a median concentration along the full GEOVIDE transect of 10.3 nM ($n = 206$). In the IB, differences were found in mid waters (Fig. 6b) between GEOVIDE (median 16.5 nM), GA04N (median 23.8 nM), and GA03 (Median 32.7 nM). These are linked to a stronger presence of MOW for GA03 and GA04N than for GEOVIDE (see Sect. 3.4.1). Below 2500 m, the median dAl concentration was lowest in the ENAB (14.4 nM) and highest in the IB (20.9 nM) associated with NEADW, with a median concentration along the full transect of 16.7 nM ($n = 134$). Deep concentrations were comparable between GEOVIDE, GA04N, GA03, and GA02 (Fig. 6b), and displayed similar concentrations on the eastern and western part of the transect as noted before by Middag et al. (2015b) at a latitude of ca. 40° N.

Remineralization versus scavenging in the North Atlantic and Labrador Sea

In the remote oligotrophic regions of the North Atlantic Ocean with enhanced Saharan dust inputs, dAl shows enhanced surface water concentrations with depletion at depth (Measures et al., 2015), typical for a scavenged-type element (Bruland et al., 2014). A scavenged-type distribution for dAl has also been described for the Pacific Ocean (Orians and Bruland, 1985). In contrast, a nutrient-type depth distribution of dAl has been reported for the Arctic Ocean (Middag et al., 2009), Mediterranean Sea (Hydes et al., 1988; Rolison et al., 2015), North Atlantic (40–50° N; Barrett et al., 2012; Measures et al., 2008), and high-latitude North Atlantic (Middag et al., 2015b) and these distributions coincided with strong correlations between dAl and $\text{Si}(\text{OH})_4$ (Hydes et al., 1988; Middag et al., 2015b, 2009; Rolison et al., 2015). Dissolved Al is thought to be removed from surface waters onto particle surfaces (Moore and Millward, 1984; Orians and Bruland, 1985), including diatom cells (Gehlen et al., 2002), and subsequently released at depth during the recycling of biogenic particles and desorption from non-biogenic particles. In our study region, diatoms dominate the phytoplankton communities at the early stage of the spring bloom (Brown et al., 2003), and are an important producer of bSi (Nelson et al., 1995). This, along with other biogenic particles, is a main carrier for scavenged Al (Moran and Moore, 1988b; Stoffyn, 1979). Elevated bSi concentrations and associated high export rates of bSi were measured using in situ pumps in the ENAB (up to 1.19 μM bSi), and in the IrB, and LB (up to 4.27 and 4.63 μM bSi, respectively; Lemaitre et al., 2018). Dissolved Al and $\text{Si}(\text{OH})_4$ displayed strong correlations (full dataset $R^2 = 0.56$, Fig. S5) with depth in all basins (ENAB, IcB, IrB and LB; $R^2 > 0.76$), except in the IB ($R^2 = 0.2$) which featured Al enrichment from the MOW (see Sect. 3.4.1), the Tagus estuary, and the Iberian shelf and margin (see Sect. 3.2.1 and 3.4.2). The large production of opal and other biogenic particles (e.g. CaCO_3 from coccolithophorids; Lemaitre et al., 2018), the strong correlation between dAl and $\text{Si}(\text{OH})_4$ with depth, and the increase in dAl concentrations with depth (Fig. 6a and b, see Sect. 3.3) suggest that in the water column the net remineralization of dAl from particles was larger than the net removal of dAl from scavenging. However, it should be noted that dAl removal by diatom production is not necessarily the only reason for the nutrient-type distribution. Whilst we did not observe enhanced pAl concentrations where coccolithophorids were dominant (e.g. IcB; Sect. 3.2.2, Fig. 2), we assume that other biogenic and non-biogenic particles (e.g. CaCO_3 , organic carbon, lithogenic particles, and zooplankton fecal pellets) will also contribute to the vertical export of surface dAl into the deep ocean. Advection and mixing of water masses with different preformed dAl concentrations will also influence water column distributions of dAl, as observed for water masses with low dAl concentrations (e.g. DSOW) in com-

parison with overlying waters (e.g. ISOW; see Sect. 3.4.2). Enhanced sediment resuspension can furthermore add dAl to bottom waters (see Sect. 3.4.2).

3.4 Dissolved Al enrichment at depth

3.4.1 Mediterranean outflow water (MOW)

The Mediterranean Sea receives large inputs of aerosols which result in elevated surface dAl concentrations of up to 174 nM, as reported by Hydes et al. (1988). The presence of the MOW was indicated by a mid-depth maximum in salinity (> 36 ; Fig. 1b), low oxygen concentrations ($< 171 \mu\text{M}$, Sarthou et al., 2018), and a dAl maximum (Fig. 6a and c) at stations 11 to 29, relative to surrounding water masses. The highest dAl concentration (38.7 nM) in the outflow water was observed at station 1 (ca. 900 m deep), in agreement with observations made along GA03 for station USGT10-1 (depth 876 m; dAl = 38.8 nM; Measures et al., 2015). Figure 8 displays dAl and pAl versus salinity in the MOW for a neutral-density surface layer (γ^n) between 27.6 and 27.8 kg m^{-3} , corresponding to a MOW core depth, based on highest salinity values, between 1000 and 1200 m. In addition, dAl versus S for cruises GA03 and GA04N are plotted. The data used in the linear regressions cover a distance of 1800 km from station 11 to station 29. The coefficients of determination (R^2) observed for dAl and pAl against salinity are 0.95 and 0.67 (Fig. 8), respectively. The linear correlation between dAl, pAl, and salinity, as well as the shape of the vertical distribution of dAl at station 11 (Fig. S4) indicate that the MOW is highly enriched in dAl and represents a major source of dAl to mid-depth waters in the North Atlantic. In addition, the good correlation between dAl and salinity, as well as the steady decline of dAl in a westerly direction along the neutral-density surface layer 27.7 kg m^{-3} , suggest that the dAl content of MOW is mainly controlled by mixing with surrounding water masses and only to a minor degree by the remineralization of biogenic particles. Due to this, dAl is a quantitative tracer for MOW.

3.4.2 Sediment resuspension

Sediment resuspension and transport due to physical forcings, such as internal waves, tides, and currents, as well as diffusion of Al-rich pore waters, are all deemed to increase Al levels in bottom waters (Stoffyn-Egli, 1982; Van Beueskom et al., 1997). Enhanced dAl levels have been observed as a result of continental margin inputs for the Drake Passage (Middag et al., 2012) and European shelf (de Jong et al., 2007; Moran and Moore, 1991). Moreover, in the North Atlantic, resuspension of sediments associated with benthic nepheloid layers has been shown to elevate dAl concentrations in comparison to overlying waters (Middag et al., 2015b; Moran and Moore, 1991; Sherrell and Boyle, 1992).

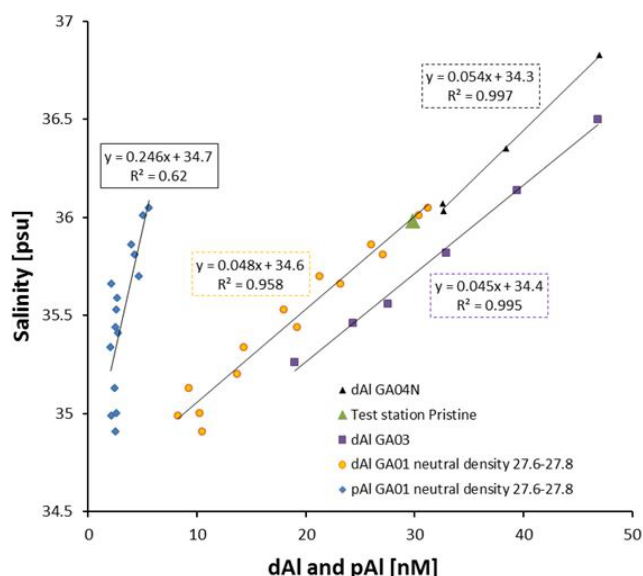


Figure 8. Dissolved Al and particulate Al (pAl; Gourain et al., 2018) concentrations against salinity for the Mediterranean Outflow Water (MOW) between the neutral-density layer 27.6 and 27.8 kg m⁻³. GA03 (Measures et al., 2015), GA04N (Rolison et al., 2015), and test station Pristine (Rijkenberg et al., 2015).

On the Iberian and Greenland shelves and margins we observed both enhanced dAl concentrations and pAl to dAl ratios (Figs. 3, 4, and 5). In contrast, on the Newfoundland shelf no enhanced dAl concentrations were observed. On the Iberian shelf and margin, enhanced dAl concentrations were observed near the seafloor (station 2: up to 21 nM at a depth of 140 m; station 4: up to 27 nM at a depth of 800 m), associated with enhanced pAl concentrations of up to 1.5 μM at station 2 (Fig. S6; Gourain et al., 2018). Likely, the Portugal Current (Coelho et al., 2002; Huthnance et al., 2002), and poleward (Frouin et al., 1990) and equatorward upper slope currents (Hall et al., 2000), caused the sediment resuspension responsible for the observed enhanced Al levels. On the Greenland margin and shelf, elevated dAl concentrations were measured at stations 53 and 61 (station 53: up to 17.4 nM at a depth of 180 m) and coincided with high pAl concentrations (up to 73.2 nM). The EGC and West Greenland Current (WGC) are known to produce sediment resuspension. Additionally, Mienert et al. (1993) showed that sediments are transported across the shelf from meltwater and runoff. In contrast, on the Newfoundland shelf and margin (station 78), no enhanced dAl levels were observed near the seafloor (Fig. S6). However, a large input of pAl was observed (station 78), and pAl concentrations increased from 94.6 nM at a depth of 140 m to 550 nM at the seafloor (377 m; Gourain et al., 2018). Dissolved Al could be scavenged by resuspended particles, thus showing lower levels where elevated pAl levels were observed. Thus, the enhanced pAl levels could be attributed to sediment resuspension events

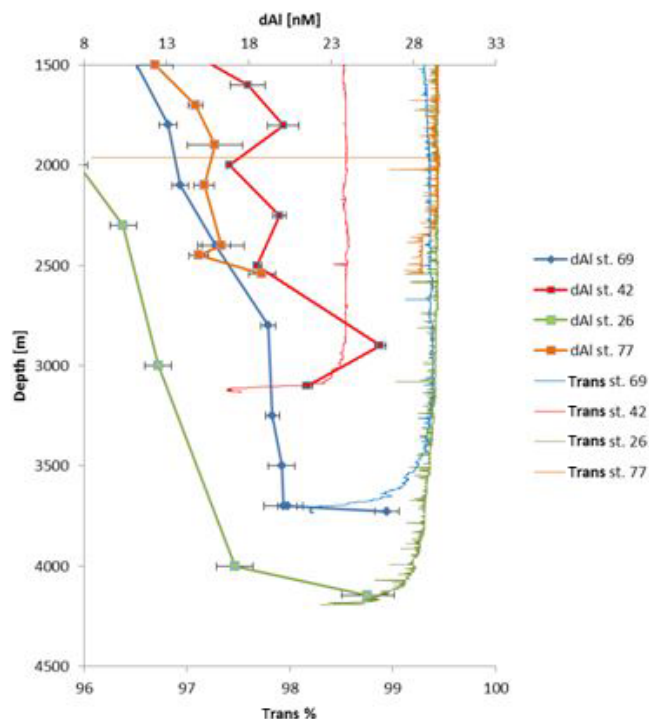


Figure 9. Dissolved Al (nM) and beam transmissometer (%) profiles for stations 26, 42, 69, and 77.

caused by the south-flowing Labrador Current (Mertz et al., 1993), possibly in combination with eddies that could also transfer terrigenous inputs into the Labrador Sea (Chanut et al., 2008; Hátún et al., 2007).

Enhanced dAl concentrations in the bottom layers of several basins (Iceland, Irminger, Labrador) accompanied by enhanced attenuation signals from the beam transmissometer were indicative of the presence of benthic nepheloid layers which are typically caused by strong bottom currents (e.g. ISOW and DSOW; Eittrheim et al., 1976). Figure 9 shows dAl and transmissometry profiles for stations 26, 42, 69, and 77 (Fig. S7 shows pAl for the same stations). Enhanced dAl concentrations near the seafloor coincided with enhanced pAl (Gourain et al., 2018) and a beam attenuation signal. In contrast, at station 42, dAl concentrations decreased near the seafloor. Based on the eOMP analysis (García Ibanez et al., 2018), the waters at 2900 m depth (dAl 25.1 nM) had an ISOW contribution of 66% and a residual contribution of DSOW of 2%. In contrast, near the seafloor, the contribution of DSOW increased to 91% with a residual ISOW contribution of 6%. Thus, the low dAl concentrations near the seafloor were probably related to low dAl DSOW in comparison with overlaying dAl-rich ISOW as reported by Middag et al. (2015b). Enhanced dAl concentrations with no concomitant decrease in transmissometry (station 77) could indicate that dAl was released from pore waters.

Overall, the observed enhanced Al concentrations suggest that along the GEOVIDE section, continental shelves and margins acted as a source of Al to adjacent waters. However, dAl concentrations did not always increase when enhanced pAl concentrations were present which implies that the release or sorption mechanisms from shelf and deep sea sediments may be different. These results suggest that, occasionally, scavenging of dAl onto resuspended particles may be a dominant process rather than partial dissolution of Al from resuspended sediments. However, the mechanisms controlling either a net dissolution or scavenging of Al from or by resuspended particles remain unclear. Moreover though, the general increase in Al concentrations in bottom layers suggests that these areas act as a potential source of Al to the North Atlantic Deep Water as observed in previous studies (Measures et al., 2015; Middag et al., 2015b; Moran and Moore, 1991).

3.4.3 Hydrothermal activity

Hydrothermal activity was assessed at station 38 over the Mid-Atlantic Ridge. Hydrothermal activity has been reported as a source of dAl to the deep ocean in the Pacific and Atlantic (Measures et al., 2015; Resing et al., 2015). No enhanced dAl (Fig. 6a) or dFe (Tonnard et al., 2018a) concentrations were evident, although Achterberg et al. (2018) observed enhanced dFe over the Reykjanes ridge and attributed this to a possible combination of hydrothermal sources and sediment resuspension. However, enhanced concentrations in particulate Al (up to 28 nM, Fig. 7), Fe, Ti, and Mn and a pFe to pAl ratio similar to the ratio in fresh mid-ocean ridge basalts were observed at station 38 (Gourain et al., 2018). Therefore, the minor pAl signature observed at station 38 could be partly related to hydrothermal inputs and resuspension of newly formed oceanic crust.

4 Conclusions

The dAl distribution in seawater is controlled by the relative strength of its sources and removal processes. At large basin scales, along the GEOVIDE section, the dAl distribution was mostly determined by low aerosol depositions, removal onto biogenic particles, and the remineralization of biogenic particles at depth. Yet we show that at smaller regional scales, local sources such as rivers and glacial runoff controlled the dAl signatures. Additionally, sediment resuspension events and the processes of sorption or desorption of dAl onto or from particles were important mechanisms determining the dAl concentrations at the sediment–water interface. Our results highlight the importance of phytoplankton (particularly diatom) abundance and dynamics for determining the interaction between dissolved and particulate Al phases in surface waters.

Overall, the Al distribution along the GEOVIDE section, in addition to other recent discoveries from the GEOTRACES programme, highlights the complex nature of dAl biogeochemical cycling in seawater as it can resemble a scavenged-type or a nutrient-type element. The large sets of parameters measured on each GEOTRACES cruise will allow us, in the coming years, to examine the global ocean dAl cycling from a holistic perspective.

Data availability. The 2014 GEOTRACES GA01 section data for dAl are available at the Intermediate Data Product 2017 (Schlitzer et al., 2018) and can be downloaded from the GEOTRACES website (<http://www.geotraces.org/dp/idp2017>).

The Supplement related to this article is available online at <https://doi.org/10.5194/bg-15-5271-2018-supplement>.

Competing interests. The authors declare that they have no conflict of interest.

Special issue statement. This article is part of the special issue “GEOVIDE, an international GEOTRACES study along the OVIDE section in the North Atlantic and in the Labrador Sea (GA01)”. It is not associated with a conference.

Acknowledgements. We are greatly thankful to the captain, Gilles Ferrand, and crew of the N/O *Pourquoi Pas?* for their help during the GEOVIDE mission. Many thanks to Tom Browning for valuable comments which helped to improve the manuscript. We would like to give a special thanks to Pierre Branellec, Michel Hamon, Catherine Kermabon, Philippe Le Bot, Stéphane Leizour, Olivier Ménage (Laboratoire de Physique des Océans et Spatiale), Fabien Pérault, and Emmanuel de Saint Léger (Division Technique de l'INSU, Brest, France) for their technical expertise during clean CTD deployments and to Catherine Schmechtig for the GEOVIDE database management. We also acknowledge Emilie Grosteffan, Manon Le Goff, Morgane Galinari, and Paul Tréguer for the analysis of nutrients. Greg Cutter is also thanked for his help in setting up the new French clean sampling system. This work was supported by GEOMAR, a PhD Fellowship of the Department of Scientific Politics of the Basque government to JLMB, the French National Research Agency (ANR-13-BS06-0014, ANR-12-PDOC-0025-01), the French National Centre for Scientific Research (CNRS-LEFE-CYBER), the LabexMER (ANR-10-LABX-19), and IFREMER. We thank the Helmholtz Association for financing the publication costs for this manuscript.

The article processing charges for this open-access publication were covered by a Research Centre of the Helmholtz Association.

Edited by: Gideon Henderson

Reviewed by: Joseph A. Resing, Rob Middag, and one anonymous referee

References

- Achterberg, E. P., Steigenberger, S., Marsay, C. M., LeMoigne, F. A., Painter, S. C., Baker, A. R., Connelly, D. P., Moore, C. M., Tagliabue, A., and Tanhua, T.: Iron Biogeochemistry in the High Latitude North Atlantic Ocean, *Sci. Rep.*, 8, 1283, <https://doi.org/10.1038/s41598-018-19472-1>, 2018.
- Aminot, A. and K erouel, R.: Dosage automatique des nutriments dans les eaux marines: m ethodes en flux continu, Editions Quae, available at: <http://www.quae.com/fr/r1172-dosage-automatiquedes-nutriments-dans-les-eaux-marines.html> (last access: 19 July 2016), 2007.
- Bacon, S., Reverdin, G., Rigor, I. G., and Snaith, H. M.: A freshwater jet on the east Greenland shelf, *J. Geophys. Res.-Oceans*, 107, 5-1–5-16, <https://doi.org/10.1029/2001JC000935>, 2002.
- Baringer, M. O. N. and Price, J. F.: Mixing and spreading of the Mediterranean outflow, *J. Phys. Oceanogr.*, 27, 1654–1677, 1997.
- Barrett, P. M., Resing, J. A., Buck, N. J., Buck, C. S., and Landing, W. M.: The trace element composition of suspended particulate matter in the upper 1000 m of the eastern North Atlantic Ocean: A16N, *Mar. Chem.*, 142, 41–53, 2012.
- Barrett, P. M., Resing, J. A., Buck, N. J., Landing, W. M., Morton, P. L., and Shelley, R. U.: Changes in the distribution of Al and particulate Fe along A16N in the eastern North Atlantic Ocean between 2003 and 2013: Implications for changes in dust deposition, *Mar. Chem.*, 177, 57–68, 2015.
- Brown, L., Sanders, R., Savidge, G., and Lucas, C. H.: The uptake of silica during the spring bloom in the Northeast Atlantic Ocean, *Limnol. Oceanogr.*, 48, 1831–1845, 2003.
- Brown, M. T. and Bruland, K. W.: An improved flow-injection analysis method for the determination of dissolved aluminum in seawater, *Limnol. Oceanogr.-Meth.*, 6, 87–95, 2008.
- Brown, M. T. and Bruland, K. W.: Dissolved and particulate aluminum in the Columbia River and coastal waters of Oregon and Washington: Behavior in near-field and far-field plumes, *Estuar. Coast. Shelf S.*, 84, 171–185, 2009.
- Brown, M. T., Lippiatt, S. M., and Bruland, K. W.: Dissolved aluminum, particulate aluminum, and silicic acid in northern Gulf of Alaska coastal waters: Glacial/riverine inputs and extreme reactivity, *Mar. Chem.*, 122, 160–175, 2010.
- Bruland, K., Middag, R., and Lohan, M.: Controls of trace metals in seawater, in: *Treatise on Geochemistry*, edited by: Holland, H. and Turekian, K., Elsevier, Amsterdam, the Netherlands, 19–51, 2014.
- Carpenter, J. H.: The accuracy of the Winkler method for dissolved oxygen analysis, *Limnol. Oceanogr.*, 10, 135–140, 1965.
- Chanut, J., Barnier, B., Large, W., Debreu, L., Penduff, T., Molines, J. M., and Mathiot, P.: Mesoscale eddies in the Labrador Sea and their contribution to convection and restratification, *J. Phys. Oceanogr.*, 38, 1617–1643, 2008.
- Chou, L. and Wollast, R.: Biogeochemical behavior and mass balance of dissolved aluminum in the western Mediterranean Sea, *Deep-Sea Res. Pt. II*, 44, 741–768, 1997.
- Coelho, H., Neves, R., White, M., Leitao, P., and Santos, A.: A model for ocean circulation on the Iberian coast, *J. Marine Syst.*, 32, 153–179, 2002.
- de Jong, J. T., Boy e, M., Gelado-Caballero, M. D., Timmermans, K. R., Veldhuis, M. J., Nolting, R. F., Van den Berg, C. M., and de Baar, H. J.: Inputs of iron, manganese and aluminium to surface waters of the Northeast Atlantic Ocean and the European continental shelf, *Mar. Chem.*, 107, 120–142, 2007.
- Duce, R., Liss, P., Merrill, J., Atlas, E., Buat-Menard, P., Hicks, B., Miller, J., Prospero, J., Arimoto, R., and Church, T.: The atmospheric input of trace species to the world ocean, *Global Biogeochem. Cy.*, 5, 193–259, 1991.
- Eittr eim, S., Thorndike, E. M., and Sullivan, L.: Turbidity distribution in the Atlantic Ocean, *Deep Sea Research and Oceanographic Abstracts*, 23, 1115–1127, 1976.
- Frouin, R., Fi uza, A. F. G., Ambar, I., and Boyd, T. J.: Observations of a poleward surface current off the coasts of Portugal and Spain during winter, *J. Geophys. Res.-Oceans*, 95, 679–691, 1990.
- Garc a-Ib a nez, M. I., P erez, F. F., Lherminier, P., Zunino, P., Mercier, H., and Tr eguer, P.: Water mass distributions and transports for the 2014 GEOVIDE cruise in the North Atlantic, *Biogeosciences*, 15, 2075–2090, <https://doi.org/10.5194/bg-15-2075-2018>, 2018.
- Gehlen, M., Beck, L., Calas, G., Flank, A.-M., Van Bennekom, A., and Van Beusekom, J.: Unraveling the atomic structure of biogenic silica: evidence of the structural association of Al and Si in diatom frustules, *Geochim. Cosmochim. Ac.*, 66, 1601–1609, 2002.
- Gourain, A., Planquette, H., Cheize, M., Lemaitre, N., Menzel Barraqueta, J.-L., Shelley, R., Lherminier, P., and Sarthou, G.: Inputs and processes affecting the distribution of particulate iron in the North Atlantic along the GEOVIDE (GEOTRACES GA01) section, *Biogeosciences Discuss.*, <https://doi.org/10.5194/bg-2018-234>, in review, 2018.
- Grand, M. M., Measures, C. I., Hatta, M., Hiscock, W. T., Landing, W. M., Morton, P. L., Buck, C. S., Barrett, P. M., and Resing, J. A.: Dissolved Fe and Al in the upper 1000 m of the eastern Indian Ocean: A high-resolution transect along 95  E from the Antarctic margin to the Bay of Bengal, *Global Biogeochem. Cy.*, 29, 375–396, 2015.
- Guerzoni, S., Molinaroli, E., and Chester, R.: Saharan dust inputs to the western Mediterranean Sea: depositional patterns, geochemistry and sedimentological implications, *Deep-Sea Res. Pt. II*, 44, 631–654, 1997.
- Hall, I., Schmidt, S., McCave, I., and Reyss, J.: Particulate matter distribution and disequilibrium along the Northern Iberian Margin: implications for particulate organic carbon export, *Deep-Sea Res. Pt. ,* 47, 557–582, 2000.
- Hall, I. R. and Measures, C.: The distribution of Al in the IOC stations of the North Atlantic and Norwegian Sea between 52  and 65  North, *Mar. Chem.*, 61, 69–85, 1998.
- Han, Q., Moore, J. K., Zender, C., Measures, C., and Hydes, D.: Constraining oceanic dust deposition using surface ocean dissolved Al, *Global Biogeochem. Cy.*, 22, GB2003, <https://doi.org/10.1029/2007GB002975>, 2008.
- H at un, H., Eriksen, C. C., and Rhines, P. B.: Buoyant eddies entering the Labrador Sea observed with gliders and altimetry, *J. Phys. Oceanogr.*, 37, 2838–2854, 2007.

- Hopwood, M. J., Connelly, D. P., Arendt, K. E., Juul-Pedersen, T., Stinchcombe, M. C., Meire, L., Esposito, M., and Krishna, R.: Seasonal changes in Fe along a glaciated Greenlandic fjord, *Front. Earth Sci.*, 4, 15, <https://doi.org/10.3389/feart.2016.00015>, 2016.
- Huthnance, J. M., Van Aken, H. M., White, M., Barton, E. D., Le Cann, B., Coelho, E. F., Fanjul, E. A., Miller, P., and Vitorino, J.: Ocean margin exchange – water flux estimates, *J. Marine Syst.*, 32, 107–137, 2002.
- Hydes, D., De Lange, G., and De Baar, H.: Dissolved aluminium in the Mediterranean, *Geochim. Cosmochim. Ac.*, 52, 2107–2114, 1988.
- Hydes, D. J.: Aluminum in seawater: Control by inorganic processes, *Science*, 205, 1260–1262, 1979.
- Hydes, D. J.: Seasonal variation in dissolved aluminium concentrations in coastal waters and biological limitation of the export of the riverine input of aluminium to the deep sea, *Cont. Shelf Res.*, 9, 919–929, 1989.
- Jeandel, C., Peucker-Ehrenbrink, B., Jones, M. T., Pearce, C. R., Oelkers, E. H., Godderis, Y., Lacan, F., Aumont, O., and Arsouze, T.: Ocean margins: The missing term in oceanic element budgets?, *Eos T. Am. Geophys. Un.*, 92, 217–218, 2011.
- Jickells, T. D., An, Z. S., Andersen, K. K., Baker, A. R., Bergametti, G., Brooks, N., Cao, J. J., Boyd, P. W., Duce, R. A., Hunter, K. A., Kawahata, H., Kubilay, N., laRoche, J., Liss, P. S., Mahowald, N., Prospero, J. M., Ridgwell, A. J., Tegen, I., and Torres, R.: Global iron connections between desert dust, ocean biogeochemistry, and climate, *Science*, 308, 67–71, 2005.
- Koning, E., Gehlen, M., Flank, A.-M., Calas, G., and Epping, E.: Rapid post-mortem incorporation of aluminum in diatom frustules: Evidence from chemical and structural analyses, *Mar. Chem.*, 106, 208–222, 2007.
- Kramer, J., Laan, P., Sarthou, G., Timmermans, K. R., and de Baar, H. J. W.: Distribution of dissolved aluminium in the high atmospheric input region of the subtropical waters of the North Atlantic Ocean, *Mar. Chem.*, 88, 85–101, 2004.
- Kremling, K.: The distribution of cadmium, copper, nickel, manganese, and aluminium in surface waters of the open Atlantic and European shelf area, *Deep-Sea Res.*, 32, 531–555, 1985.
- Kremling, K. and Hydes, D.: Summer distribution of dissolved Al, Cd, Co, Cu, Mn and Ni in surface waters around the British Isles, *Cont. Shelf Res.*, 8, 89–105, 1988.
- Lannuzel, D., Bowie, A. R., van der Merwe, P. C., Townsend, A. T., and Schoemann, V.: Distribution of dissolved and particulate metals in Antarctic sea ice, *Mar. Chem.*, 124, 134–146, 2011.
- Lemaître, N., Planchon, F., Planquette, H., Dehairs, F., Fonseca-Batista, D., Roukaerts, A., Deman, F., Tang, Y., Mariez, C., and Sarthou, G.: High variability of export fluxes along the North Atlantic GEOTRACES section GA01: Particulate organic carbon export deduced from the ^{234}Th method, *Biogeosciences Discuss.*, <https://doi.org/10.5194/bg-2018-190>, in review, 2018.
- Longhurst, A. R.: *Ecological geography of the sea*, Academic Press, Elsevier, 560 pp., 2010.
- Mahowald, N. M., Baker, A. R., Bergametti, G., Brooks, N., Duce, R. A., Jickells, T. D., Kubilay, N., Prospero, J. M., and Tegen, I.: Atmospheric global dust cycle and iron inputs to the ocean, *Global Biogeochem. Cy.*, 19, GB4025, <https://doi.org/10.1029/2004GB002402>, 2005.
- Maring, H. B. and Duce, R. A.: The impact of atmospheric aerosols on trace metal chemistry in open ocean surface seawater, I. Aluminium, *Earth Planet. Sc. Lett.*, 84, 381–392, 1987.
- Martin, T. and Wadhams, P.: Sea-ice flux in the East Greenland Current, *Deep-Sea Res. P. II*, 46, 1063–1082, 1999.
- Mawji, E., Schlitzer, R., Dodas, E. M., Abadie, C., Abouchami, W., Anderson, R. F., Baars, O., Bakker, K., Baskaran, M., Bates, N. R., Bluhm, K., Bowie, A., Bown, J., Boye, M., Boyle, E. A., Branallec, P., Bruland, K. W., Brzezinski, M. A., Bucciarelli, E., Buesseler, K., Butler, E., Cai, P., Cardinal, D., Casciotti, K., Chaves, J., Cheng, H., Chever, F., Church, T. M. and Colman, A. S., Conway, T. M., Croot, P. L., Cutter, G. A., de Baar, H. J. W., de Souza, G. F., Dehairs, F., Deng, F., Dieu, H. T., Dulaquais, G., Echevoyen-Sanz, Y., Lawrence Edwards, R., Fahrback, E., Fitzsimmons, J., Fleisher, M., Frank, M., Friedrich, J., Fripiat, F., Galer, S. J. G., Gamo, T., Solsona, E. G., Gerringa, L. J. A., Godoy, J. M., Gonzalez, S., Grossteffan, E., Hatta, M., Hayes, C. T., Heller, M. I., Henderson, G., Huang, K.-F., Jeandel, C., Jenkins, W. J., John, S., Kenna, T. C., Klunder, M., Kretschmer, S., Kumamoto, Y., Laan, P., Labatut, M., Lacan, F., Lam, P. J., Lannuzel, D., le Moigne, F., Lechtenfeld, O. J., Lohan, M. C., Lu, Y., Masqué, P., McClain, C. R., Measures, C., Middag, R., Moffett, J., Navidad, A., Nishioka, J., Noble, A., Obata, H., Ohnemus, D. C., Owens, S. and Planchon, F., Pradoux, C., Puigcorbé, V., Quay, P., Radic, A., Rehkämper, M., Remenyi, T., Rijkenberg, M. J. A., Rintoul, S., Robinson, L. F., Roeske, T., Rosenberg, M., van der Loeff, M. R., Ryabenko, E., Saito, M. A., Roshan, S., Salt, L., Sarthou, G., Schauer, U., Scott, P., Sedwick, P. N., Sha, L., Shiller, A. M., Sigman, D. M., Smethie, W., Smith, G. J., Sohrin, Y., Speich, S., Stichel, T., Stutsman, J., Swift, J. H., Tagliabue, A., Thomas, A., Tsunogai, U., Twining, B. S., van Aken, H. M., van Heuven, S. and van Ooijen, J., van Weerlee, E., Venchiarutti, C., Voelker, A. H. L., Wake, B., Warner, M. J., Woodward, E. M. S., Wu, J., Wyatt, N., Yoshikawa, H. and Zheng, X.-Y., Xue, Z., Zieringer, M., and Zimmer, L. A.: The GEOTRACES Intermediate Data Product 2014, *Mar. Chem.*, 177, 1–8, 2015.
- Measures, C. and Edmond, J.: Aluminium in the South Atlantic: steady state distribution of a short residence time element, *J. Geophys. Res.-Oceans*, 95, 5331–5340, 1990.
- Measures, C. and Vink, S.: On the use of dissolved aluminum in surface waters to estimate dust deposition to the ocean, *Global Biogeochem. Cy.*, 14, 317–327, 2000.
- Measures, C., Grant, B., Khadem, M., Lee, D., and Edmond, J.: Distribution of Be, Al, Se and Bi in the surface waters of the western North Atlantic and Caribbean, *Earth Planet. Sci. Lett.*, 71, 1–12, 1984.
- Measures, C., Edmond, J., and Jickells, T.: Aluminium in the north-west Atlantic, *Geochim. Cosmochim. Ac.*, 50, 1423–1429, 1986.
- Measures, C., Brown, M., and Vink, S.: Dust deposition to the surface waters of the western and central North Pacific inferred from surface water dissolved aluminum concentrations, *Geochem. Geophys. Geosy.*, 6, Q09M03, <https://doi.org/10.1029/2005GC000922>, 2005.
- Measures, C., Landing, W., Brown, M., and Buck, C.: High-resolution Al and Fe data from the Atlantic Ocean CLIVAR-CO2 Repeat Hydrography A16N transect: Extensive linkages between atmospheric dust and upper ocean geochemistry, *Global Biogeochem. Cy.*, 22, GB1005, <https://doi.org/10.1029/2007GB003042>, 2008.

- Measures, C., Hatta, M., Fitzsimmons, J., and Morton, P.: Dissolved Al in the zonal N Atlantic section of the US GEOTRACES 2010/2011 cruises and the importance of hydrothermal inputs, *Deep-Sea Res. Pt. II*, 116, 176–186, 2015.
- Measures, C. I. and Brown, E. T.: Estimating Dust Input to the Atlantic Ocean Using Surface Water Aluminium Concentrations, in: *The Impact of Desert Dust Across the Mediterranean*, edited by: Guerzoni, S. and Chester, R., Springer Netherlands, Dordrecht, the Netherlands, 1996.
- Menzel Barraqueta, J.-L., Klar, J. K., Gledhill, M., Schlosser, C., Shelley, R., Planquette, H., Wenzel, B., Sarthou, G., and Achterberg, E. P.: Atmospheric aerosol deposition fluxes over the Atlantic Ocean: A GEOTRACES case study, *Biogeosciences Discuss.*, <https://doi.org/10.5194/bg-2018-209>, in review, 2018.
- Mertz, G., Narayanan, S., and Helbig, J.: The freshwater transport of the Labrador Current, *Atmos. Ocean*, 31, 281–295, 1993.
- Middag, R., de Baar, H. J. W., Laan, P., and Bakker, K.: Dissolved aluminium and the silicon cycle in the Arctic Ocean, *Mar. Chem.*, 115, 176–195, 2009.
- Middag, R., van Slooten, C., de Baar, H. J. W., and Laan, P.: Dissolved aluminium in the Southern Ocean, *Deep-Sea Res. Pt. II*, 58, 2647–2660, 2011.
- Middag, R., Baar, H. d., Laan, P., and Huhn, O.: The effects of continental margins and water mass circulation on the distribution of dissolved aluminum and manganese in Drake Passage, *J. Geophys. Res.-Oceans*, 117, C01019, <https://doi.org/10.1029/2011JC007434>, 2012.
- Middag, R., Séférian, R., Conway, T., John, S., Bruland, K., and de Baar, H.: Intercomparison of dissolved trace elements at the Bermuda Atlantic Time Series station, *Mar. Chem.*, 177, 476–489, <https://doi.org/10.1016/j.marchem.2015.06.014>, 2015a.
- Middag, R., Van Hulst, M., Van Aken, H., Rijkenberg, M., Gerringa, L., Laan, P., and De Baar, H.: Dissolved aluminium in the ocean conveyor of the West Atlantic Ocean: effects of the biological cycle, scavenging, sediment resuspension and hydrography, *Mar. Chem.*, 177, 69–86, 2015b.
- Mienert, J., Thiede, J., Kenyon, N., and Hollender, F. J.: Polar continental margins: studies off East Greenland, *EOS T. Am. Geophys. Un.*, 74, 225–236, 1993.
- Moore, R. M. and Millward, G. E.: Dissolved-particulate interactions of aluminium in ocean waters, *Geochim. Cosmochim. Ac.*, 48, 235–241, 1984.
- Moran, S. and Moore, R.: Temporal variations in dissolved and particulate aluminum during a spring bloom, *Estuar. Coast. Shelf S.*, 27, 205–215, 1988a.
- Moran, S. B. and Moore, R. M.: Evidence from mesocosm studies for biological removal of dissolved aluminium from sea water, *Nature*, 335, 706–708, 1988b.
- Moran, S. B. and Moore, R. M.: The potential source of dissolved aluminum from resuspended sediments to the North Atlantic Deep Water, *Geochim. Cosmochim. Ac.*, 55, 2745–2751, 1991.
- Nelson, D. M., Tréguer, P., Brzezinski, M. A., Leynaert, A., and Quéguiner, B.: Production and dissolution of biogenic silica in the ocean: revised global estimates, comparison with regional data and relationship to biogenic sedimentation, *Global Biogeochem. Cy.*, 9, 359–372, 1995.
- Orians, K. J. and Bruland, K. W.: Dissolved aluminium in the central North Pacific, *Nature*, 316, 427–429, 1985.
- Orians, K. J. and Bruland, K. W.: The biogeochemistry of aluminum in the Pacific Ocean, *Earth Planet. Sc. Lett.*, 78, 397–410, 1986.
- Planquette, H. and Sherrell, R. M.: Sampling for particulate trace element determination using water sampling bottles: methodology and comparison to in situ pumps, *Limnol. Oceanogr. Meth.*, 10, 367–388, 2012.
- Pollard, R. T., Griffiths, M. J., Cunningham, S. A., Read, J. F., Pérez, F. F., and Ríos, A. F.: Vivaldi 1991 – A study of the formation, circulation and ventilation of Eastern North Atlantic Central Water, *Prog. Oceanogr.*, 37, 167–192, 1996.
- Prospero, J. M. and Carlson, T. N.: Vertical and areal distribution of Saharan dust over the western equatorial North Atlantic Ocean, *J. Geophys. Res.*, 77, 5255–5265, 1972.
- Read, J.: CONVEX-91: water masses and circulation of the North-east Atlantic subpolar gyre, *Prog. Oceanogr.*, 48, 461–510, 2000.
- Resing, J. A. and Measures, C. I.: Fluorometric Determination of Al in Seawater by Flow Injection Analysis with In-Line Preconcentration, *Anal. Chem.*, 66, 4105–4111, 1994.
- Resing, J. A., Sedwick, P. N., German, C. R., Jenkins, W. J., Moffett, J. W., Sohst, B. M., and Tagliabue, A.: Basin-scale transport of hydrothermal dissolved metals across the South Pacific Ocean, *Nature*, 523, 200–203, 2015.
- Rijkenberg, M. J. A., de Baar, H. J. W., Bakker, K., Gerringa, L. J. A., Keijzer, E., Laan, M., Laan, P., Middag, R., Ober, S., van Ooijen, J., Ossebaar, S., van Weerlee, E. M., and Smit, M. G.: “PRISTINE”, a new high volume sampler for ultraclean sampling of trace metals and isotopes, *Mar. Chem.*, 177, 501–509, 2015.
- Roberson, C. E. and Hem, J. D.: Solubility of aluminum in the presence of hydroxide, fluoride, and sulfate, *Water Supply Paper 1827-C*, USGPO, <https://doi.org/10.3133/wsp1827C>, 1969.
- Rolison, J., Middag, R., Stirling, C., Rijkenberg, M., and De Baar, H.: Zonal distribution of dissolved aluminium in the Mediterranean Sea, *Mar. Chem.*, 177, 87–100, 2015.
- Rudnick, R. and Gao, S.: *Treatise on Geochemistry*, vol. 3, edited by: Rudnick, R. L., Holland, H. D., and Turekian, K. K., Elsevier, 1–64, <https://doi.org/10.1016/B0-08-043751-6/03016-4>, 2003.
- Sarthou, G., Lherminier, P., Achterberg, E. P., Alonso-Pérez, F., Bucciarelli, E., Boutorh, J., Bouvier, V., Boyle, E. A., Branellec, P., Carracedo, L. I., Casacuberta, N., Castrillejo, M., Cheize, M., Contreira Pereira, L., Cossa, D., Daniault, N., De Saint-Léger, E., Dehairs, F., Deng, F., Desprez de Gésincourt, F., Devesa, J., Foliot, L., Fonseca-Batista, D., Gallinari, M., García-Ibáñez, M. I., Gourain, A., Grossteffan, E., Hamon, M., Heimbürger, L. E., Henderson, G. M., Jeandel, C., Kermabon, C., Lacan, F., Le Bot, P., Le Goff, M., Le Roy, E., Lefèbvre, A., Leizour, S., Lemaitre, N., Masqué, P., Ménage, O., Menzel Barraqueta, J.-L., Mercier, H., Perault, F., Pérez, F. F., Planquette, H. F., Planchon, F., Roukaerts, A., Sanial, V., Sauzède, R., Shelley, R. U., Stewart, G., Sutton, J. N., Tang, Y., Tisnérat-Laborde, N., Tonnard, M., Tréguer, P., van Beek, P., Zurbrick, C. M., and Zunino, P.: Introduction to the French GEOTRACES North Atlantic Transect (GA01): GEOVIDE cruise, *Biogeosciences Discuss.*, <https://doi.org/10.5194/bg-2018-312>, in review, 2018.
- Schlitzer, R.: Ocean Data View, available at: <http://odv.awi.de>, last access: 1 January 2018.
- Schlitzer, R., Anderson, R. F., Dodas, E. M., Lohan, M., Geibert, W., Tagliabue, A., Bowie, A., Jeandel, C., Maldonado, M. T., Landing, W. M., Cockwell, D., Abadie, C., Abouchami, W.,

- Achterberg, E. P., Agather, A., Aguiar-Islas, A., van Aken, H. M., Andersen, M., Archer, C., Auro, M., de Baar, H. J., Baars, O., Baker, A. R., Bakker, K., Basak, C., Baskaran, M., Bates, N. R., Bauch, D., van Beek, P., Behrens, M. K., Black, E., Bluhm, K. and Bopp, L., Bouman, H., Bowman, K., Bown, J., Boyd, P., Boye, M., Boyle, E. A., Branellec, P., Bridgestock, L., Brissebrat, G., Browning, T., Bruland, K. W., Brumsack, H.-J., Brzezinski, M., Buck, C. S., Buck, K. N., Buesseler, K. and Bull, A., Butler, E., Cai, P., Mor, P. C., Cardinal, D., Carlson, C., Carrasco, G., Casacuberta, N., Casciotti, K. L., Castrillejo, M., Chamizo, E. and Chance, R., Charette, M. A., Chaves, J. E., Cheng, H., Chever, F., Christl, M., Church, T. M., Closset, I., Colman, A., Conway, T. M., Cossa, D. and Croot, P., Cullen, J. T., Cutter, G. A., Daniels, C., Dehairs, F., Deng, F., Dieu, H. T., Duggan, B., Dulaquais, G., Dumousseaud, C., Echevoyen-Sanz, Y., Edwards, R. L., Ellwood, M., Fahrback, E., Fitzsimmons, J. N., Russell Flegal, A., Fleisher, M. Q., van de Fliedert, T., Frank, M., Friedrich, J., Fripiat, F., Fröllje, H., Galer, S. J. G., Gamo, T., Ganeshram, R. S., Garcia-Orellana, J., Garcia-Solsona, E., Gault-Ringold, M., George, E., Gerringa, L. J. A., Gilbert, M., Godoy, J. M., Goldstein, S. L., Gonzalez, S. R., Grissom, K., Hammerschmidt, C., Hartman, A., Hassler, C. S., Hathorne, E. C., Hatta, M., Hawco, N., Hayes, C. T., Heimbürger, L.-E., Helgoe, J., Heller, M., Henderson, G. M., Henderson, P. B., van Heuven, S., Ho, P., Horner, T. J., Hsieh, Y.-T., Huang, K.-F., Humphreys, M. P., Ishiki, K., Jacquot, J. E., Janssen, D. J., Jenkins, W. J., John, S., Jones, E. M., Jones, J. L., Kadko, D. C., Kayser, R., Kenna, T. C., Khondoker, R., Kim, T. and Kipp, L., Klar, J. K., Klunder, M., Kretschmer, S., Kumamoto, Y., Laan, P., Labatut, M., Lacan, F., Lam, P. J., Lambelet, M., Lamborg, C. H., Le Moigne, F. A. C., Le Roy, E., Lechtenfeld, O. J., Lee, J.-M., Lherminier, P. and Little, S., López-Lora, M., Lu, Y., Masque, P., Mawji, E., McClain, C. R., Measures, C., Mehic, S., Barraqueta, J.-L. M., van der Merwe, P., Middag, R., Mieruch, S., Milne, A., Minami, T., Moffett, J. W., Moncoiffe, G. and Moore, W. S., Morris, P. J., Morton, P. L., Nakaguchi, Y., Nakayama, N. and Niedermiller, J., Nishioka, J., Nishiuchi, A., Noble, A., Obata, H., Ober, S., Ohnemus, D. C., van Ooijen, J., O'Sullivan, J., Owens, S., Pahnke, K., Paul, M., Pavia, F., Pena, L. D., Peters, B., Planchon, F., Planquette, H., Pradoux, C., Puigcorbè, V., Quay, P., Queroue, F., Radic, A., Rauschenberg, S., Rehkämper, M., Rember, R., Remenyi, T., Resing, J. A. and Rickli, J., Rigaud, S., Rijkenberg, M. J. A., Rintoul, S., Robinson, L. F., Roca-Martí, M., Rodellas, V., Roeske, T., Rolison, J. M., Rosenberg, M., Roshan, S., Rutgers van der Loeff, M. M., Ryabenko, E., Saito, M. A., Salt, L. A., Sanial, V., Sarthou, G., Schallenberg, C., Schauer, U., Scher, H., Schlosser, C., Schnetger, B., Scott, P., Sedwick, P. N., Semiletov, I. and Shelley, R., Sherrell, R. M., Shiller, A. M., Sigman, D. M., Singh, S. K. and Slagter, H. A., Slater, E., Smethie, W. M., Snaith, H., Sohrin, Y., Sohst, B., Sonke, J. E., Speich, S., Steinfeldt, R., Stewart, G., Stichel, T. and Stirling, C. H., Stutsman, J., Swarr, G. J., Swift, J. H., Thomas, A., Thorne, K., Till, C. P., Till, R., Townsend, A. T., Townsend, E., Tuerena, R. and Twining, B. S., Vance, D., Velazquez, S., Venchiarutti, C., Villa-Alfageme, M., Vivancos, S. M., Voelker, A. H. L., Wake, B., Warner, M. J., Watson, R., van Weerlee, E., Alexandra Weigand, M., Weinstein, Y., Weiss, D., Wisotzki, A., Woodward, E. M. S., Wu, J., Wu, Y., Wuttig, K., Wyatt, N. and Xiang, Y., Xie, R. C., Xue, Z., Yoshikawa, H., Zhang, J., Zhang, P., Zhao, Y., Zheng, L., Zheng, X.-Y., Zieringer, M., Zimmer, L. A., Ziveri, P., Zunino, P., and Zurbrück, C.: The GEOTRACES Intermediate Data Product 2017, *Chem. Geol.*, 493, 210–223, <https://doi.org/10.1016/j.chemgeo.2018.05.040>, 2018 (data available at: <http://www.geotraces.org/dp/idp2017>, last access: 19 July 2017).
- Schlosser, C., Klar, J. K., Wake, B. D., Snow, J. T., Honey, D. J., Woodward, E. M. S., Lohan, M. C., Achterberg, E. P., and Moore, C. M.: Seasonal ITCZ migration dynamically controls the location of the (sub)tropical Atlantic biogeochemical divide, *P. Natl. Acad. Sci.*, 111, 1438–1442, 2014.
- Schlosser, C., Schmidt, K., Aquilina, A., Homoky, W. B., Castrillejo, M., Mills, R. A., Patey, M. D., Fielding, S., Atkinson, A., and Achterberg, E. P.: Mechanisms of dissolved and labile particulate iron supply to shelf waters and phytoplankton blooms off South Georgia, Southern Ocean, *Biogeosciences Discuss.*, <https://doi.org/10.5194/bg-2017-299>, in review, 2017.
- Shelley, R. U., Morton, P. L., and Landing, W. M.: Elemental ratios and enrichment factors in aerosols from the US-GEOTRACES North Atlantic transects, *Deep-Sea Res. Pt. II*, 116, 262–272, 2015.
- Shelley, R. U., Roca-Martí, M., Castrillejo, M., Masqué, P., Landing, W. M., Planquette, H., and Sarthou, G.: Quantification of trace element atmospheric deposition fluxes to the Atlantic Ocean (> 40° N; GEOVIDE, GEOTRACES GA01) during spring 2014, *Deep-Sea Res. Pt. I*, 119, 34–49, 2017.
- Sherrell, R. M. and Boyle, E. A.: The trace metal composition of suspended particles in the oceanic water column near Bermuda, *Earth Planet. Sc. Lett.*, 111, 155–174, 1992.
- Statham, P. J., Skidmore, M., and Tranter, M.: Inputs of glacially derived dissolved and colloidal iron to the coastal ocean and implications for primary productivity, *Global Biogeochem. Cy.*, 22, GB3013, <https://doi.org/10.1029/2007GB003106>, 2008.
- Stoffyn, M.: Biological control of dissolved aluminum in seawater: experimental evidence, *Science*, 203, 651–653, 1979.
- Stoffyn, M. and Mackenzie, F. T.: Fate of dissolved aluminum in the oceans, *Mar. Chem.*, 11, 105–127, 1982.
- Stoffyn-Egli, P.: Dissolved aluminium in interstitial waters of recent terrigenous marine sediments from the North Atlantic Ocean, *Geochim. Cosmochim. Ac.*, 46, 1345–1352, 1982.
- Sutherland, D. A., Pickart, R. S., Peter Jones, E., Azetsu-Scott, K., Jane Eert, A., and Ólafsson, J.: Freshwater composition of the waters off southeast Greenland and their link to the Arctic Ocean, *J. Geophys. Res.-Oceans*, 114, C05020, <https://doi.org/10.1029/2008JC004808>, 2009.
- Swift, J. H., Aagaard, K., and Malmberg, S.-A.: The contribution of the Denmark Strait overflow to the deep North Atlantic, *Deep-Sea Res.*, 27, 29–42, 1980.
- Talley, L. D. and McCartney, M. S.: Distribution and Circulation of Labrador Sea Water, *J. Phys. Oceanogr.*, 12, 1189–1205, 1982.
- Tanhua, T., Olsson, K. A., and Jeansson, E.: Formation of Denmark Strait overflow water and its hydro-chemical composition, *J. Marine Syst.*, 57, 264–288, 2005.
- Tonnard, M., Planquette, H., Bowie, A. R., van der Merwe, P., Gallinari, M., Desprez de Gésincourt, F., Germain, Y., Gourain, A., Benetti, M., Reverdin, G., Tréguer, P., Boutorh, J., Cheize, M., Menzel Barraqueta, J.-L., Pereira-Contreira, L., Shelley, R., Lherminier, P., and Sarthou, G.: Dissolved iron in the North Atlantic Ocean and Labrador Sea along the GEOVIDE sec-

- tion (GEOTRACES section GA01), *Biogeosciences Discuss.*, <https://doi.org/10.5194/bg-2018-147>, in review, 2018a.
- Tonnard, M., Donval, A., Lampert, L., Claustre, H., Ras, J., Dimier, C., Sarthou, G., Planquette, H., van der Merwe, P., Boutorh, J., Cheize, M., Menzel Barraqueta, J.-L., Pereira Contraira, L., Shelley, R., Bowie, A. R., Tréguer, P., Gallinari, M., Duprez de Gesincourt, F., Germain, Y., and Lherminier, P.: Phytoplankton assemblages along the GEOVIDE section (GEOTRACES section GA01) using CHEMTAX, in preparation, 2018b.
- Ussher, S. J., Achterberg, E. P., Powell, C., Baker, A. R., Jickells, T. D., Torres, R., and Worsfold, P. J.: Impact of atmospheric deposition on the contrasting iron biogeochemistry of the North and South Atlantic Ocean, *Global Biogeochem. Cy.*, 27, 1096–1107, <https://doi.org/10.1002/gbc.20056>, 2013.
- Van Aken, H. and De Boer, C.: On the synoptic hydrography of intermediate and deep water masses in the Iceland Basin, *Deep-Sea Res. Pt. I*, 42, 165–189, 1995.
- van Bennekom, A. J.: On the role of aluminium in the dissolution kinetics of diatom frustules, in: *Proc. 6th Diatom Symposium 1980*, Koeltz, Koenigsten, edited by: Ross, R., 445–455, 1981.
- Van Beueskom, J., Van Bennekom, A., Tréguer, P., and Morvan, J.: Aluminium and silicic acid in water and sediments of the Enderby and Crozet Basins, *Deep-Sea Res. Pt. II*, 44, 987–1003, 1997.
- van Hulten, M. M. P., Sterl, A., Tagliabue, A., Dutay, J. C., Gehlen, M., de Baar, H. J. W., and Middag, R.: Aluminium in an ocean general circulation model compared with the West Atlantic Geotraces cruises, *J. Marine Syst.*, 126, 3–23, 2013.
- van Hulten, M. M. P., Sterl, A., Middag, R., de Baar, H. J. W., Gehlen, M., Dutay, J.-C., and Tagliabue, A.: On the effects of circulation, sediment resuspension and biological incorporation by diatoms in an ocean model of aluminium*, *Biogeosciences*, 11, 3757–3779, <https://doi.org/10.5194/bg-11-3757-2014>, 2014.
- Vink, S. and Measures, C. I.: The role of dust deposition in determining surface water distributions of Al and Fe in the South West Atlantic, *Deep-Sea Res. Pt. II*, 48, 2787–2809, 2001.
- Vrieling, E. G., Poort, L., Beelen, T. P., and Gieskes, W. W.: Growth and silica content of the diatoms *Thalassiosira weissflogii* and *Navicula salinarum* at different salinities and enrichments with aluminium, *Eur. J. Phycol.*, 34, 307–316, 1999.
- Woodgate, R. A., Fahrbach, E., and Rohardt, G.: Structure and transports of the East Greenland Current at 75 N from moored current meters, *J. Geophys. Res.-Oceans*, 104, 18059–18072, 1999.